Optical and electronic properties of Si nanoclusters synthesized in inverse micelles

J. P. Wilcoxon, G. A. Samara, and P. N. Provencio
Sandia National Laboratories, Albuquerque, New Mexico 87185-1421
(Received 10 December 1998; revised manuscript received 31 March 1999)

Highly crystalline, size-selected silicon (Si) nanocrystals in the size range 2–10 nm were grown in inverse micelles and their optical absorption and photoluminescence (PL) properties were studied. High resolution TEM and electron diffraction results show that these nanocrystals retain their cubic diamond structures down to sizes ~4 nm in diameter, and optical absorption data suggest that this structure and bulklike properties are retained down to the smallest sizes produced (~1.8 nm diameter containing about 150 Si atoms). High pressure liquid chromatography techniques with on-line optical and electrical diagnostics were developed to purify and separate the clusters into pure, monodisperse populations. The optical absorption revealed features associated with both the indirect and direct band-gap transitions, and these transitions exhibited different quantum confinement effects. The indirect band-gap shifts from 1.1 eV in the bulk to ~2.1 eV for nanocrystals ~2 nm in diameter and the direct transition at $\Gamma(\Gamma_{25}-\Gamma_{15})$ blueshifts by 0.4 eV from its 3.4 eV bulk value over the same size range. Tailorable, visible, room temperature PL in the range 700–350 nm (1.8–3.5 eV) was observed from these nanocrystals. The most intense PL was in the violet region of the spectrum (~365 nm) and is attributed to direct electron-hole recombination. Other less intense PL peaks are attributed to surface state and to indirect band-gap recombination. The results are compared to earlier work on Si clusters grown by other techniques and to the predictions of various model calculations. Currently, the wide variations in the theoretical predictions of the various models along with considerable uncertainties in experimental size determination for clusters less than 3–4 nm, make it difficult to select among competing models. [S0163-1829(99)02328-0]

I. INTRODUCTION

Because it is an indirect band-gap semiconductor, silicon (Si) has a major drawback: its inability to emit light efficiently, and, furthermore, its weak emission is in the near IR. There is presently a large research effort aimed at exploring physical and chemical means to break silicon's lattice symmetry and mix different momentum (k) states in order to induce a useful level of luminescence and optical gain. The approaches include[1] (1) impurity-induced luminescence (e.g., S, B, Be, Er), (2) alloy-induced luminescence (e.g., Si-Ge-C), (3) porous silicon, and (4) quantum wires and dots (or nanosize clusters). The first two of these approaches are plagued by, among other things, relatively low luminescence intensity at low temperature which becomes vanishingly weak at room temperature, whereas the last two, which may be mechanistically related via quantum confinement, have considerable potential but have remained largely uncontrolled and poorly understood. Success in this endeavor is obviously a major challenge to materials science, one that could have profound technological implications.

Because visible photoluminescence (PL) has been observed from Si nanoclusters,[1] these clusters and their potential are a subject of current interest. Si nanoclusters have been produced by aerosol techniques,[2] plasma deposition,[3] sputtering,[4] spark ablation[5] and grown as colloids,[6] or in glass matrices by a variety of approaches[7–9] including ion implantation[9] followed by high temperature annealing; however, all of these techniques produce a large distribution of cluster sizes resulting in very broad optical absorption and PL features which limit usefulness and make definitive interpretation in terms of quantum confinement and other mechanisms difficult.

To understand the origin of visible PL and other electronic properties of Si nanoclusters, it is necessary to study size-selected nanoclusters and to assess the role of surface recombination. Definitive experimental results will be key to future scientific progress and practical utilization of this material. From a physics perspective, such studies should lead to a better understanding of quantum confinement of electrons and holes in indirect band-gap semiconductors. Quantum confinement in direct gap semiconductors such as GaAs and CdSe is fairly well understood, but much less is known about confinement in indirect gap materials.[10–11] The bulk excitonic radius for Si is ~4 nm which suggests that quantum confinement effects should be observed for nanocrystals smaller than this size.

We have developed a synthesis method based on using inverse micelles as reaction vessels[12] to produce useful quantities of size-selected clusters and have used this method to synthesize a variety of metal and compound semiconductor clusters.[13–15] These clusters have been remarkable in their size monodispersity and the sharpness and richness of their spectral features which have demonstrated strong quantum confinement effects. In this paper we apply our inverse micellar synthesis method to produce size-selected Si nanoclusters and to study their size-dependent optical absorption and photoluminescence (PL). We shall first discuss the synthesis and characterization of these nanoclusters and then present and discuss their optical properties including comparison with earlier work and theoretical predictions.

II. SYNTHESIS AND CHARACTERIZATION

Size-selected nanosize Si clusters were grown by a generic process described in detail elsewhere.[12,13] Controlled

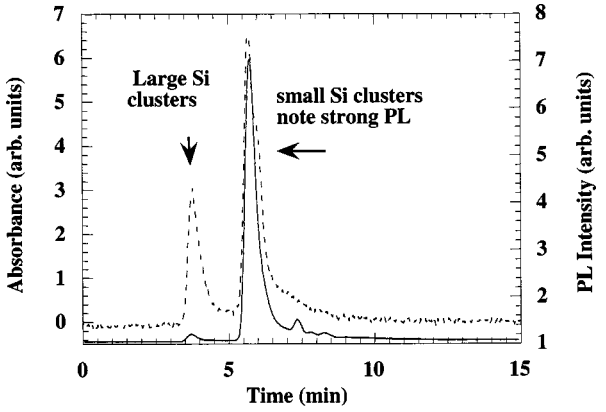

FIG. 1. Coplot of optical absorbance at 250 nm (dashed line) and PL (emission detector at 400 nm excitation at 250 nm, solid line) vs elution time for a solution containing two sizes of Si nanocrystals. Chromatography conditions were a ODS200-c18 (c18-terminated reverse phase) column with 120 Å pores, using acetonitrile as a mobile phase at 0.5 ml/min flow.

nucleation and growth of the nanoclusters occurs in the interior of nanosize surfactant aggregates called inverse micelles. An anhyrous ionic salt (e.g., SiX_4, where $X=$Cl, Br, or I is dissolved in the hydrophilic interior of a solution of micelles. Since the ionic salts are completely insoluble in the continuous oil medium used (e.g., octane), nucleation and growth of Si is restricted to the micelle interior which can be varied from 1–10 nm. The anhydrous salt dissolves to form a transparent ionic solution but with a complete absence of water; in a sense the salt is ''hydrated'' by the micelle. The absence of water prevents simple hydrolysis to form SiO_2 which is why this synthesis must be performed in water-free oils like octane or decane, and using a controlled atmosphere glove box. Similarly, the surfactants used, both nonionic aliphatic polyethers, or alternatively quaternary ammonium cationic surfactants, must be dissolved in anhydrous THF and dried over Na metal to remove any small traces of water.

We next reduce Si(IV) to Si(0) using an anhydrous metal hydride, (usually 1 M $LiAlH_4$ in THF). The reduction is rapid with vigorous bubbling as H_2 gas is released, electrons are transferred to the Si(IV) and the light yellow solution becomes clear (for the smallest clusters formed). One can determine the correct stoichiometry of the reaction by following the disappearance of the Si(IV) charge transfer peaks from the precursor solution. Control over cluster size is achieved by variation of the micelle size, intermicellar interactions and reaction chemistry. Clusters with diameters between 1.8 and ~10 nm were produced. Spectroscopy and high pressure liquid chromatography (HPLC) with on-line spectroscopy, conductivity and refractive index diagnostics were used to demonstrate 100% reduction of the Si(IV) to the final Si(0) nanocluster form. All solvents and surfactants used were HPLC grade and completely dust free to prevent inhomogeneous nucleation.

Since there is no source of oxygen in the reaction mixture, and anhydrous metal hydrides are used as reducing agents, it is likely that the Si cluster surface is terminated by hydrogen from the metal hydride, although we currently have no direct proof of this. When kept in the glove box under Ar, there appears to be no long term (i.e., 6 month to 1 year) degradation of the Si nanoclusters. However, upon exposure to oxygen, a yellowing of the solution occurs presumably due to surface oxidization.

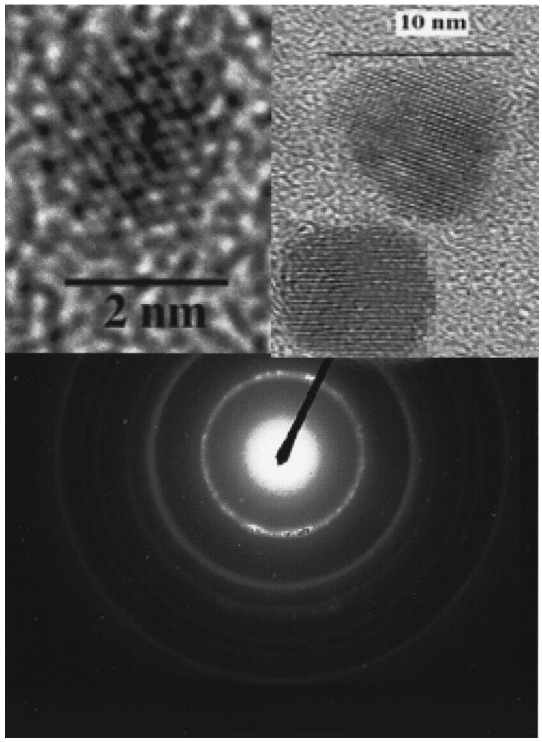

FIG. 2. HRTEM images of a 2 nm Si crystal (upper left), 8–10 nm crystals (upper right), and a SAD pattern for 8–10 nm crystals.

HPLC separation and elution peak spectral data were obtained using apparatus with automated fraction collection. Previous HPLC experiments on Si/SiO_2 nanoclusters synthesized in the gas phase showed a broad range of elution times[2,10] which is in contrast with our results where the Si peak is of comparable width to that from the other molecular constituents of the solution. Figure 1 illustrates separation of two sizes of Si nanoclusters. Using the PL detector we can identify which size of cluster has significant room temperature PL, and also make sure that no impurity organic chemicals could be giving rise to the PL signal. Only the absorbance peak corresponding to the more numerous population of small, 2.0 nm clusters coincides with a strong visible PL signal. We also obtained the complete absorbance and PL wavelength dependences for each size Si nanoclusters as will be shown in Sec. III. Inductively coupled plasma/mass spectroscopy of the collected Si fractions showed that nearly 80% of the total Si was recovered by HPLC and the only inorganic detected was Si. Gas chromatography/mass spectroscopy showed the only significant organic chemical in the collected fractions was the mobile phase solvent. In particular, no surfactant was detected.

Other characterization tools employed were x-ray diffraction, selected area electron diffraction (SAD), and high-resolution transmission electron microscopy (HRTEM). Figure 2 shows HRTEM images of a 2 nm crystal (upper left), 8–10 nm crystals (upper right) and a SAD pattern from 8–10 nm crystals. The high crystalline quality is evident.

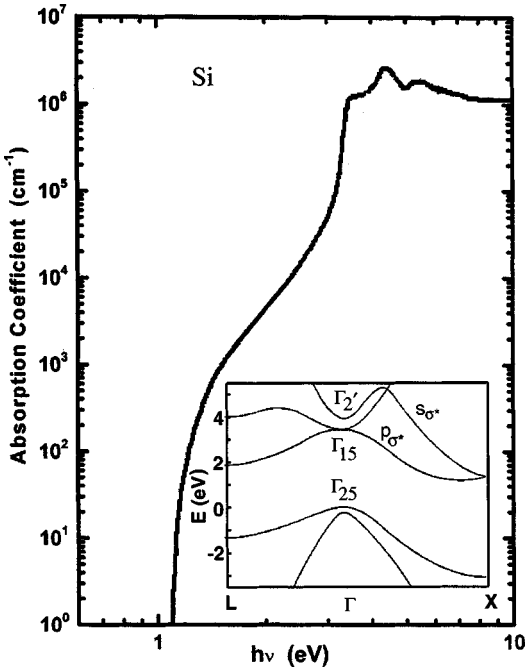

FIG. 3. The optical absorption spectrum of bulk Si at 300 K (after Ref. 16) and the band structure near the band-gap region (after Ref. 17).

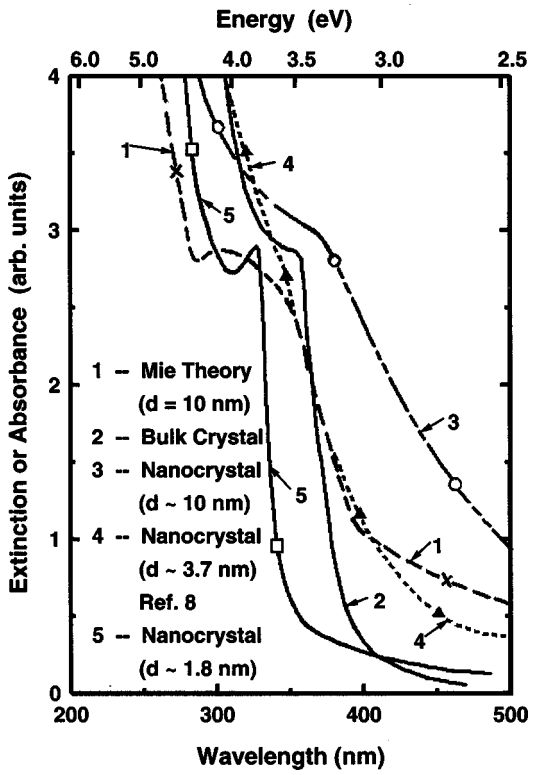

FIG. 4. The extinction spectra of several Si nanocrystal samples compared with the absorption spectrum of bulk Si and a Mie theory calculation for $d=10$ nm Si taken from Ref. 10.

III. RESULTS AND DISCUSSIONS

A. Optical absorption

To better understand the optical absorption of Si clusters, it is instructive to review the spectrum of bulk Si,[16] which reflect the details of the band structure[17] (Fig. 3). The long absorption tail between 1.2 and ~3 eV reflects the indirect nature of the bandgap. The sharp rise in absorption with increasing photon energy starting around 3.2 eV (380 nm) is associated with the direct transition at the Γ point [$\Gamma_{25} \rightarrow \Gamma_{15}$] whose energy is 3.4 eV (365 nm), and the second sharp rise starting around 4 eV (320 nm) is associated with a second direct transition, most likely the $\Gamma_{25}-\Gamma_{2'}$ transition whose energy is 4.2 eV (295 nm) or possibly the direct transition at X.

The measured optical response (or extinction) of nanocrystals reflects the sum of the scattering and absorption. The scattering needs to be taken into consideration in comparing cluster spectra to that of bulk Si. Figure 4 shows the extinction spectrum of relatively large ($d=10$ nm) Si clusters calculated[2,10] from Mie theory and compares it to the absorption spectrum of bulk Si. The two spectra are normalized around the absorption shoulder corresponding to the $\Gamma_{25} \rightarrow \Gamma_{15}$ direct transition. One of the obvious differences in the two spectra is the significantly enhanced extinction of the clusters which is due to scattering. Shown also in Fig. 4 are three cluster spectra (also normalized at about the shoulder of the $\Gamma_{25} \rightarrow \Gamma_{15}$ transition), two ($d=10$ and 1.8 nm) from the present work and the third ($d=3.7$ nm) from Kanemitsu's work.[8] Our $d=10$ nm spectrum is from one of our earliest samples that was not purified and size-separated by HPLC, and thus we suspect that it had a relatively broad size distribution. Because of uncertainties in the absolute values of the measured extinction coefficients, the normalization of the nanocrystal spectra in Fig. 4 is only approximate and is merely intended to reveal the shape and influence of scattering, leaving the discussion of the details of the cluster spectra until later.

Some of our Si nanocrystal samples exhibited considerable structure in their absorption spectra while others had less structure. Featureless spectra have been observed by other workers from Si nanocrystals embedded in glass matrices or from surface oxidized nanocrystals. However, subtle features are sometimes observed. The results of Littau *et al.*[2(a)] on the larger ($d=6.5$ nm) of their two samples exhibit a weak hint of the direct-gap absorptions at ~360 nm and at ~290 nm. Similarly, there is an inflection point in the absorbance in Kanemitsu's data[8] at ~350 nm. We have seen this feature in the absorbance data on several of our samples. A particularly interesting example for $d=8-10$ nm nanocrystals is shown in Fig. 5 where the feature appears as a shoulder at ~370 nm followed by a relatively sharp increase in absorbance and double peaks at ~270 nm and 220 nm. The resemblance of these features and closeness in λ to those in the spectrum of bulk Si (see Fig. 3) is striking indicating that clusters of this size ($d=8-10$ nm), which is comparable to the size of the excitonic diameter in the bulk, retain much of the character of bulk Si with very little evidence for quantum confinement effects.

Some of our smaller size nanocrystal samples exhibited highly structured absorption spectra. An example is shown in Fig. 6 for a sample with $d=2.0$ nm. The figure also shows the bulk Si spectrum for comparison. The two spectra are remarkably similar with that of the nanoclusters shifted to shorter (higher) wavelength (energy). The long absorption tail associated with the indirect band gap and the two direct

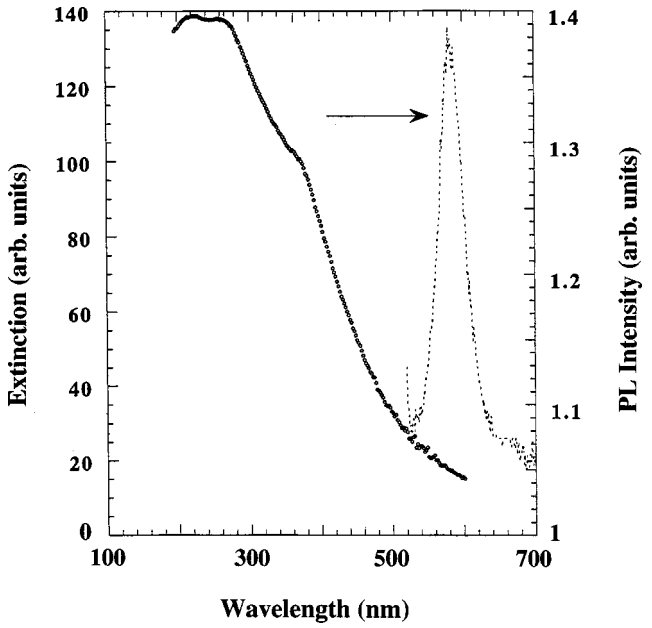

FIG. 5. The extinction and PL (excitation at 490 nm) spectra for a $d=8-10$ nm Si nanocrystal sample.

transitions ($\Gamma_{25}\rightarrow\Gamma_{15}$ and $\Gamma_{25}\rightarrow\Gamma_{2'}$ or possibly that at X) are very well defined in the nanocrystal spectrum. Because our samples are very dilute ($\sim 10^{-4}$ molar) the signal-to-noise ratio for this sample is low for the low absorbance associated with the indirect transitions, hence the noise in this region of the spectrum.

Figure 7 provides a linear absorbance vs. wavelength plot for the same two samples as in Fig. 6 with emphasis on the region of the direct transitions. The absorbances have been normalized as before to the value at the shoulder associated with the $\Gamma_{25}\rightarrow\Gamma_{15}$ transition. The close resemblance of the two spectra shows that the bulk-like character of the band structure of Si is preserved down to the $d\approx 2$ nm size (i.e., down to nanocrystals with $\sim$200 atoms or less). The data in Fig. 7 show clear evidence for quantum confinement; specifically, both direct transitions of the nanocrystals are blueshifted by about 0.4 eV compared to the bulk. As we shall see below, this is a smaller quantum confinement effect than is found for the indirect gap, but it is larger than is predicted by model calculations.

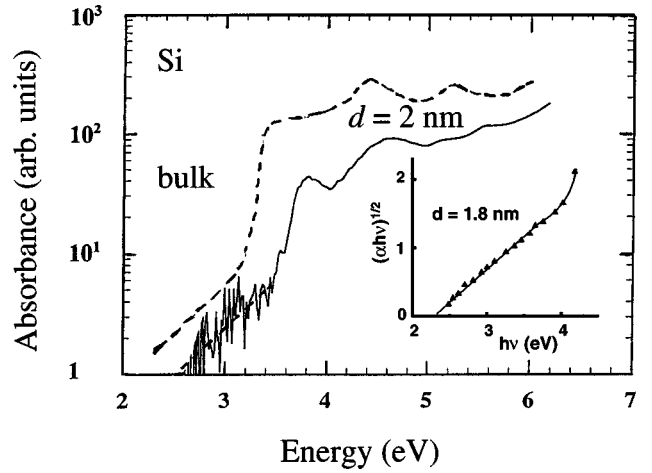

FIG. 6. The absorption spectrum of a $d=2$ nm Si nanocrystal sample. The spectrum of bulk Si is shown for comparison. The inset shows absorption results for $d=1.8$ nm Si nanocrystals. The intercept of the straight line with the x axis defines the indirect band-gap energy.

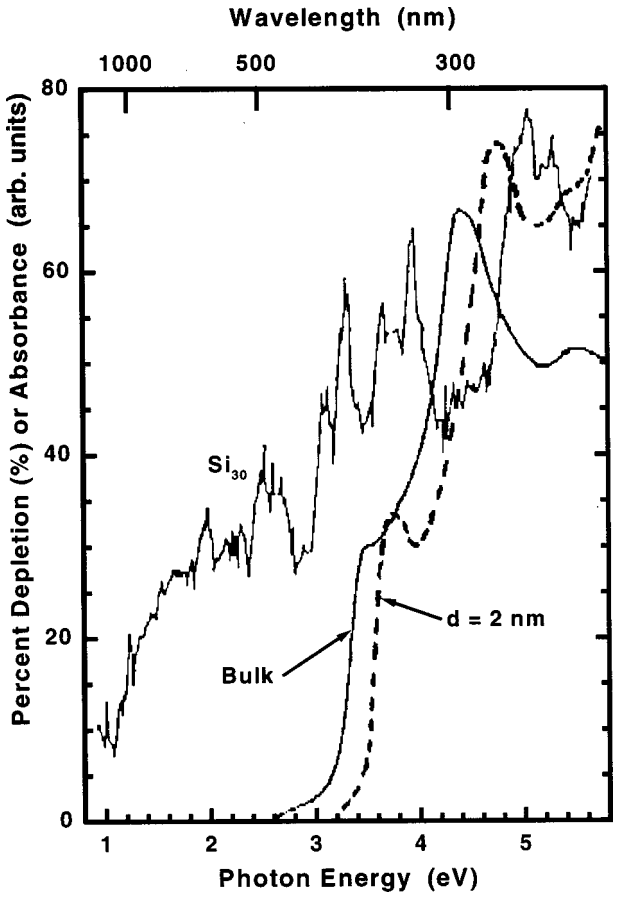

FIG. 7. The photodissociation spectrum of Si_{30} clusters from Ref. 25 is coplotted with the absorption (or extinction) spectra for bulk Si and one of our ($d=2$ nm) nanocrystal samples.

There is another aspect of the results in Fig. 7 that deserves attention. Reference to Fig. 3 reminds us that the Si conduction band at Γ involves two overlapping bands of $p_{\sigma *}$ states, one with positive and the other with negative dispersion. Quantum size confinement can be expected to influence these two bands differently resulting in their splitting which in turn might be reflected in the shape of the $\Gamma_{25}\rightarrow\Gamma_{15}$ absorption. While model calculations[18] do indeed predict such splitting, our cluster results in Fig. 7 and for other samples do not reveal it. However, our result[19] and those of others[20] on Ge nanocrystals do show evidence for such splitting.

The absorption data in Figs. 4–7 suggest a blueshift of the indirect absorption tail with decreasing nanocrystal size, and the gap appears to remain indirect. The small absorbance values in the tail region along with some uncertainty due to correcting the data for the scattering contribution make detailed analysis of the data in this wavelength region uncertain. However, the quality of the data on some of our samples was sufficiently good to allow meaningful analysis. For an indirect transition the absorption data in the region of the band edge can be described by[21] $\alpha h = C(h\nu - E_g)^2$ where α is the absorption coefficient, $h\nu$ is the photon energy, C is a constant and E_g is the band-gap energy. Analysis

of data for $d=1.8$ nm clusters using this relationship (inset in Fig. 6) yielded $E_g=2.2$ eV. While the uncertainty in this value may be as large as $\pm(0.2\text{-}0.3)$ eV because of the aforementioned weak absorption of the cluster solutions in the tail region as well as some inaccuracies introduced in correcting for scattering, the result clearly demonstrates a significant quantum confinement effect for the indirect gap of Si. Our result is in close agreement with a study by Brus *et al.*[2(b)] on SiO_2-capped Si nanocrystals. From photoluminescence excitation (PLE) and photoluminescence (PL) measurements on nanoclusters estimated to have a Si core diameter in the range 1–2 nm, these authors deduced a bandgap of 2.06 eV. As we shall discuss later, these measured quantum confinement effects are smaller than those predicted by effective mass theory but are comparable to results of some model calculations.

Our smallest Si nanocrystals ($d=1.8$ nm) have ~150 atoms and still retain bulklike optical properties. There has been considerable theoretical interest in the structure, shape and properties of Si clusters containing up to few tens atoms and in answering the question of how small can Si clusters be and still retain bulklike properties.[22–24] The results have revealed major changes in shape as a function of size with a qualitative change from prolate to more spherical structures in the narrow range between 24 and 30 atoms.[22].

Rinnen and Mandich[25] determined the absorption spectra of gas-phase neutral Si clusters in the size range Si_{18} to Si_{41} using resonant one-and two-color photodissociation spectroscopy. A surprising aspect of their results is that the spectra are essentially identical over the whole size range studied, despite the theoretical findings that there is a wide variation in the structure of the clusters over this range. The spectrum of Si_{30} is shown and compared to bulk and $d=2$ nm cluster spectra in Fig. 7. The authors observed that the Si_{18-41} spectra have much in common with the spectrum of bulk crystalline Si, however, the similarity in the spectra is not so obvious.

On the basis of their results Rinnen and Mandich[25] concluded that these small Si clusters must share one or more common structural entities which are strong chromophores. One possibility is that these small clusters share a common bonding network which persists and extends as the cluster grows in size, and that this network may be related to that of bulk Si. Another possibility is that all of these clusters contain at least one loosely bound smaller cluster such as the abundant Si_{10} which may be responsible for the sharp spectral structure in Fig. 7. We believe that the latter explanation is the correct one and offer the following explanation.

In the photodissociation experiments[25] the temperature of the clusters was estimated to be in the range 700–900 K. In work on metallic and semiconducting clusters, it is generally found that the melting point is substantially depressed with decreasing cluster size. Thus, for example, the melting point of CdSe decreases sharply with decreasing cluster size, its value for $d=3$ nm being about one half of its bulk value and is expected to be much less for smaller clusters.[11] Thus, we suggest that for the conditions of Rinnen and Mandich's experiments, their Si clusters are essentially in a ''molten state'' and that small entities like Si_{10} are indeed the dominant species. These entities have closed shape configurations[26] which can quite conceivably exist in a loosely-bound, liquidlike state. We shall return below to a discussion of the spectra of small Si nanocrystals and to a comparison of our results to theory.

B. Photoluminesence

1. Present results

The fate of photogenerated electron-hole pairs in a semiconductor is determined by traps and intrinsic recombination processes. Weak photoluminescence (PL) from phonon-assisted, indirect band-gap e-h recombination in bulk Si has been observed.[27] At room temperature, this PL peaks in the near IR at 1130 nm (=1.1 eV), and at low temperatures (e.g., 77 K) there is also emission from, or to, shallow impurity levels. In the present work on Si nanocrystals we have observed room temperature emission at various wavelengths in the range 700–350 nm (~1.8–3.5 eV), i.e., across the visible range. All our data were obtained at room temperature (295 K) and the solvent was in almost all cases acetonitrile.

In nanocrystals, a large number of the atoms are at or near the surface leading to a preponderance of dangling bonds and defects which result in surface states. Adsorbed impurities can produce additional surface states, and all of these states can act as traps or recombination sites. Consequently, light emission from nanostructures, be they nanocrystals or porous Si, can be quite complex with considerable uncertainties about the origin of the observed PL. In solution-grown nanocrystals such as our own, there is the added concern that excess precursors and reaction products can lead to some luminescence which can interfere with that due to the Si clusters. In this regard, HPLC separation/purification has led to significant improvement in the quality of the observed PL spectra. Even so, it is difficult to definitively rule out the role of contaminants in the measured PL spectra of nanoclusters in colloidal solutions.

In considering optical absorption and PL spectra it is necessary to take into account the exciton binding energy, E_B. For nanocrystals E_B is expected to be significantly enhanced over its bulk value due to quantum confinement and the expected smaller $\in$ of the nanocrystals. For example, Zunger and Wang[28] find $\in \approx 8$ for $d=2$ nm Si nanocrystals compared with a bulk value of 11.4. The smaller $\in$ also strengthens the Coulombic e-h attraction which is given by $U(r)=-e^2/\in r$, where r is the distance between the electron and hole. Tight binding calculations by Leung and Whalley[29] yield a large increase in E_B of Si with decreasing cluster size. Similarly, Takagahara and Takeda[30] calculated a large increase in E_B with decreasing cluster size for indirect-gap semiconductors in the framework of effective mass theory. Their results for Si show that E_B increases from 14.3 meV for the bulk to ~250 meV for $d=2$ nm clusters.

Figure 8 shows a room temperature PL spectrum of one of our earliest nanocrystal samples ($d\leqslant 5$ nm) obtained before developing our HPLC capability. For excitation at 256 nm, the PL spectrum exhibits intense, structured emission centered at ~365 nm (3.4 eV) and a weaker, also structured, emission centered at 600 nm (2.06 eV). It may well be that the structure in both emissions is associated with the presence of impurities or even different size populations. The 365 nm emission appears to be largely due to direct e-h recombination at $\Gamma(\Gamma_{25}-\Gamma_{15})$, and its high intensity and

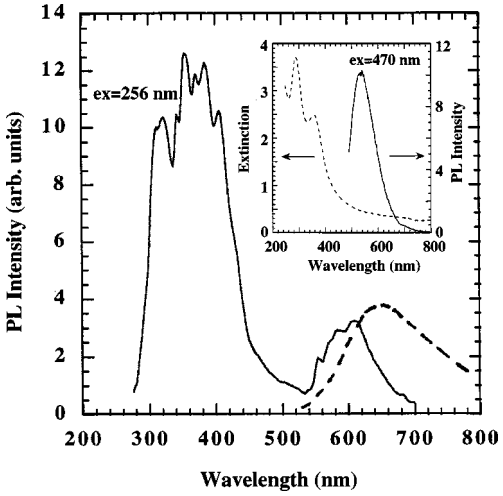

FIG. 8. The PL spectrum of an as-prepared $d \leqslant 5$ nm Si nanocrystal sample. The dashed curve is for $d < 5$ nm Si nanoclusters capped by SiO_2 excited at 350 nm, taken from Ref. 2. The inset shows a coplot of the extinction and PL spectra for a $d = 4.0$ nm Si nanocrystal sample.

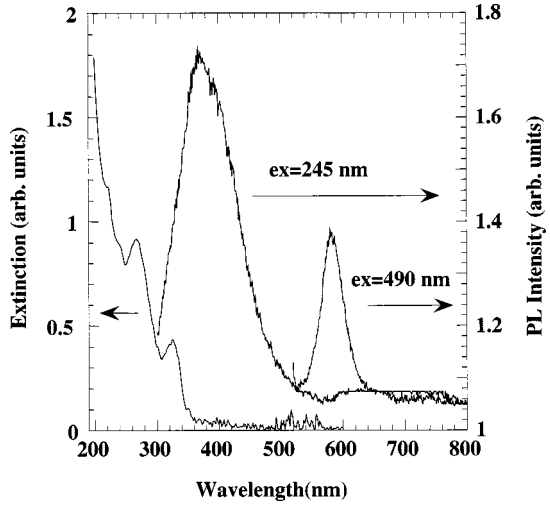

FIG. 9. Coplot of the extinction and PL spectra (for two excitation wavelengths) for $d = 2$ nm Si nanocrystal samples.

short PL decay lifetime ($\tau = 1.5$ ns, as will be discussed later) are consistent with this assignment. The origin of the 600 nm PL is more uncertain. If both emissions were intrinsic properties of Si nanocrystals, then the 600 nm emission would be due to bandgap recombination. In this scenario, reference to the absorption data discussed above, would suggest that the 365 and 600 nm emission peaks are associated with a small nanocrystal population with $d \cong 2$ nm.

The dashed curve in Fig. 8 is the PL spectrum of SiO_2-capped Si nanoclusters reported by Littau *et al.*[2(a)] for their ''1.0 colloid'' sample ($d < 5$ nm) excited at 350 nm. We believe that this luminescence has the same origin as that peaked at ~600 nm in our spectrum, but is red shifted because of larger crystallite size. As will be discussed later, we believe this luminescence is due to band gap indirect recombination.

For excitation at 320 nm the PL spectrum for our sample in Fig. 8 retains its structured two-peak character, but the peaks are red shifted compared to excitation at 256 nm. Specifically, the more intense emission is centered at ~380 nm (3.3 eV) and the less intense emission is peaked at ~680 nm (1.82 eV). The redshift of the emission may come from exciting a population of larger clusters with the longer wavelength excitation. The ~680 nm peak in our PL spectrum excited at 320 nm is redshifted from Littau *et al.*'s[2] PL spectrum in Fig. 8, consistent with a larger cluster population.

Results on a $d = 2$ nm size-selected, purified sample are shown in Fig. 9. The absorption spectrum was discussed earlier (Figs. 6 and 7). The first absorption peak at 325 nm (3.81 eV) is attributed to the $\Gamma_{25} - \Gamma_{15}$ direct gap, but blueshifted by ~0.4 eV due to quantum confinement. Excitation at 245 nm yields the PL spectrum shown. The major peak is centered at 365 nm (=3.40 eV) i.e., essentially at the same wavelength as for the sample in Fig. 8. Again, we attribute this peak to direct e-h recombination at Γ. It is redshifted from the absorption peak by 0.4 eV. It is tempting to view this shift as a measure the exciton binding energy. Indeed, its magnitude is comparable to values deduced from model calculations for Si and attributed to quantum confinement and reduced electronic screening. As we have already noted, Takagahara and Takeda[30] find $E_B > 0.25$ eV for the indirect gap of Si clusters with $d \leqslant 2$ nm. Tagaki *et al.*[3] deduced a value of $E_B = 0.32$ eV for $d \approx 3.3$ nm Si clusters. Similarly, Read *et al.*[31] find $E_B = 0.32$ eV for the indirect gap of Si quantum wires of ~3 nm diameter. More recent first principles calculations by Ögüt *et al.*[32(a)] show E_B increasing from 0.3 eV for $d = 3$ nm to ~1.0 eV for $d = 1$ nm. However, before concluding that the shift between absorption and emission peaks is equal to E_B, caution is in order. For small nanocrystals the electron and hole will be in very close proximity and the exciton state should be strong in both absorption and emission suggesting that the shift should be small.[32(b)] Thus, some uncertainty remains as to the origin of the observed 0.4 eV shift. Possible contributors are size polydispensity, electronic fine structure and/or phonon effects.

It can be seen that the major PL peak in Fig. 9 is asymmetric. Analysis of the spectrum reveals a secondary peak at ~420 nm (~3.0 eV). As appears to be typical for Si nanostructures, the 365 nm peak (with the 420 nm peak subtracted) is fairly broad, its width at half max being ~1 eV. This sample also exhibits weaker and quite broad emission at wavelengths longer than 500 nm, as shown. This luminescence is less well defined than that for the sample in Fig. 8. In addition to being purer, the sample in Fig. 9 is also more monodisperse as suggested by its sharper absorption features. Consistent with this observation, the extra structure in the PL spectrum in Fig. 8, attributed to different size populations of nanocrystals, is absent in Fig. 9.

Figure 9 also shows the PL spectrum for a similar sample excited at 490 nm (2.53 eV) i.e., just above the indirect gap for this nanocrystal size. This PL peak is centered at 580 nm (2.14 eV), and it is tempting to attribute it to indirect bandgap recombination. However, we note that this luminescence is identical to that observed on much larger ($d \cong 8-10$ nm) nanocrystals as shown in Fig. 5. We are thus led to conjecture that this PL is due to surface or defect recombination. The independence of this luminescence of nanocrystal size may be relevant to semiempirical tight-binding and ab initio local density calculations by Allan *et al.*[33] which demon-

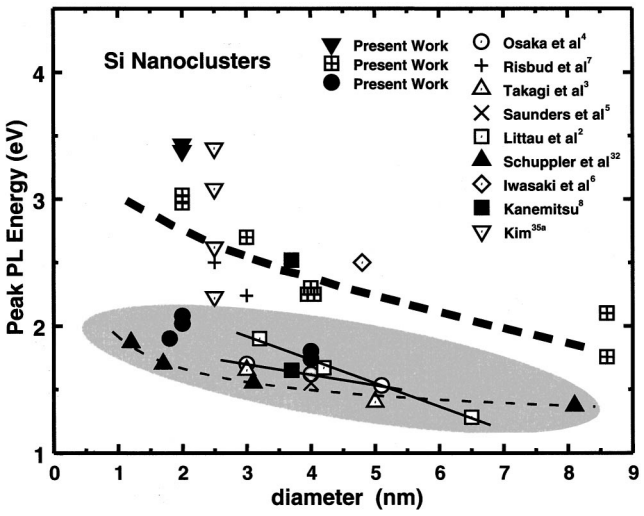

FIG. 10. Summary of data (literature and present work) on peak PL energy versus Si nanocrystal size.

strated the stability of self-trapped excitons at the surface of Si nanocrystals. The excitons are obtained for dimer bonds passivated by, e.g., hydrogen (relevant to our clusters) or silicon oxide. Light emission from these trapped excitons is essentially independent of size.

The inset in Fig. 8 shows the absorption and PL spectra of a nanocrystal sample ($d=4$ nm) with structured absorption [peaks at 355 nm (3.48 eV) and 280 nm (4.40 eV) which we believe are associated with the quantum confinement-shifted two direct transitions at Γ] exhibited a PL peak centered at 540 nm (2.30 eV) for excitation at 470 nm (2.64 eV), i.e., well below the first direct transition at Γ. This emission is at slightly shorter wavelength than the peaks in Figs. 5 and 9 suggesting extrinsic origin. The PL spectrum in the inset in Fig. 8 also has a secondary peak at $\sim$700 nm ($\sim$1.8 eV) which is most likely due to recombination at the indirect band gap.

2. Comparison with earlier luminescence results

As seen above, Si nanocrystals in solvents produced by our inverse micellar synthesis photoluminesce at various wavelengths in the range $\sim$700–350 nm ($\sim$1.8–3.6 eV). Figure 10 summarizes the results for our samples and compares the PL peak energies with those from other authors. In doing this comparison it is necessary to caution that a major uncertainty in the figure is knowledge of the size of the nanocrystals. We have presented the data using the nominal diameters deduced from our work and reported by the various authors. It is very difficult to be certain that TEM images will give truly representative dimensions and shapes in the absence of large statistical samples. In the few cases where statistical analyses were performed, it was found that nanocrystal samples embody a broad distribution of sizes. These broad distributions are evident to some extent in the very broad PL peaks of nanocrystal Si samples. Even for our HPLC-separated and purified cluster populations, we find relatively broad PL peaks, suggesting, at least in part, size dispersion. Undoubtedly, the most accurate size information in Fig. 10 is that due to Schuppler *et al.*[34] who deduced the sizes of their SiO_2-capped nanocrystals from Si*K* near-edge x-ray absorption fine structure (NEXAFS) and extended x-ray absorption fine structure (EXAFS) measurements.

Keeping in mind the above precautions, we can now offer some observations on the data in Fig. 10. Looking first at the results of earlier work, we note that there are differences in the dependence on size reported by different authors. Some of the differences, but not all, are almost certainly due to uncertainties in size. Secondly, we note that essentially all of the PL peaks energies on Si nanocrystals capped with SiO_2 or embedded in glass matrices fall within the shaded region in Fig. 10, albeit this region embodies a wide band of energies or wavelengths at each value of *d*. An issue for these samples[2,3,7,8,35(a)] is the role of the SiO_2 or glass and suboxide layer that almost certainly exists at the interface. There are undoubtedly defects and surface states at this interface, and they could play a significant role in determining the luminescence from such samples.[33] The authors of most of these works imply generally that the observed PL is intrinsic to the Si nanocrystal cores, but doubts remain. The shaded region also embodies much of the published PL peak energies on porous Si samples, an observation that has been used by some authors to suggest that the PL of porous Si is intrinsic to Si nanostructures. Strong doubts and many puzzles remain in this area as well.[2(a),35(b)]

Whereas some of our data points fall in the shaded region in Fig. 10, the rest fall well above this region. As noted earlier, our PL spectra generally exhibited a higher energy major peak and a lower energy minor peak. It is the energies of these minor peaks that fall in the shaded region. Our highest energy points in the figure are, we believe, associated with direct ($\Gamma_{25}-\Gamma_{15}$) recombination. As far as we know, this is the first observation of such direct recombination from Si and is made possible by quantum confinement. Consistent with this conclusion, the decay lifetime of the luminescence is on the order of a nanosecond (as discussed below). Kim's highest energy point in Fig. 10 may also be due to this direct recombination.

The heavy dashed curve in Fig. 10 depicts the intermediate part of our data, and the data of Kanemitsu[8] and Iwasaki *et al.*[6] Here two scenarios can be examined. The first presumes that the low energy emissions (and thereby all emissions in the lower shaded region) are due to Si bandgap emission, i.e., indirect recombination. The intermediate energy emissions would then be associated with some chromophore that may be related to the synthesis. The measured PL decay lifetimes for these emissions are on the order of a few to tens of nanoseconds, as we shall see later. Alternatively, the intermediate energy emissions are due to bandgap emissions and the low energy emissions due to surface-state recombination as also suggested by Kanemitsu.[8] The electron-hole pairs are generated in the interior of the Si nanocrystals. Some of the electrons rapidly decay into the lower-energy surface states while some (a larger fraction in our case) recombine with the holes across the gap. One difficulty with this scenario is that some of the emission energies for sizes $d>4$ nm fall above effective mass (EMA) prediction (discussed below) which overestimates the quantum confinement effect—an observation that argues in favor of the first scenario.

Some observations on porous Si are relevant to the intermediate energy regime in Fig. 10. Blue light emission is

commonly observed from aged and or oxidized porous Si. This emission is observed in the range 410–490 nm (~3.0–2.5 eV) depending on the aging/oxidation conditions, and the radiative lifetime is in the ns range for some samples and in the μs range for other samples. The energy range of this PL overlaps most of the data in the intermediate regime in Fig. 10. The origin of this PL is a subject of continuing debate between two competing mechanisms. In one, as in the recent work of Li *et al.*,[35(c)] the PL with μs lifetime is believed to come from the crystalline cores of oxidized nanometer-size Si particles, whereas the PL with ns lifetime is attributed to the oxidized layer. In the second mechanism, the PL is attributed to e-h recombination at centers located at the interface between the Si nanocrystals and the Si oxide as well as on the inside of the oxide layers.[35(d)] In this mechanism, the photoexcitation most likely occurs in the crystalline Si cores and the carriers transfer to the luminescent centers at the interface or in the oxide. This second mechanism comes closer to our present case where we believe that the PL in the intermediate regime is due to surface state recombination.

3. Radiative recombination rate and quantum efficiency

The radiative e-h recombination rate $(1/\tau)$, where τ is the radiative lifetime, is an important measure of the effectiveness of a luminescing material. For direct band gap semiconductors like GaAs the recombination is fast, τ being on the order of 1–10 nanoseconds or less. For indirect gap materials like Si, on the other hand, the recombination is slow, τ being on the order of tens of microseconds to milliseconds. In nanocrystals all vibronic as well as recombination rates are expected to increase as the electron and hole wave functions become more compact and more overlapping with decreasing size.

We have obtained τ for a couple of our Si nanocrystal samples from PL decay measurements at 295 K. The first experiment was performed on $d=3$ nm nanocrystals in solvent using an apparatus with picosecond resolution in the laboratory of our collaborator Professor David Kelley of Colorado State University. The results expressed as PL amplitude vs time at 460 nm for excitation at 300 nm are shown in Fig. 11. The decay is multiexponential but can be satisfactorily fitted by two lifetimes, a fast initial component with $\tau=46$ ps and a slow component with $\tau=1.6$ ns. It is not clear what the origin of the fast component is, but the slower is comparable to that for direct-like e-h recombination as in bulk GaAs. The inset in Fig. 11 shows the PL decay kinetics for another sample with $d=3$ nm measured at lower time resolution. The decay (for PL at 440 nm) can be adequately fit by two exponentials. The fast component with $\tau=17$ ns is convolved by the instrument response so that the decay of the sample may be actually faster. The slow component with $\tau=48$ ns is due to the sample. The scatter at long times is due to digitization noise. As discussed above, the origin of this PL is not known, but we believe it is due to surface state recombination. This $\tau=48$ ns is also much shorter than τ's observed for SiO_2-capped Si nanoclusters; e.g., Littau *et al.*[2] fit their time-resolved PL results on their colloid 1.0 sample ($d<5$ nm) with two exponentials yielding $\tau_1=17\,\mu$s and $\tau_2=76\,\mu$s. (A note of caution is in order: in Fig. 11 the decay is measured over a very narrow range of times and the τ's should be considered tentative.)

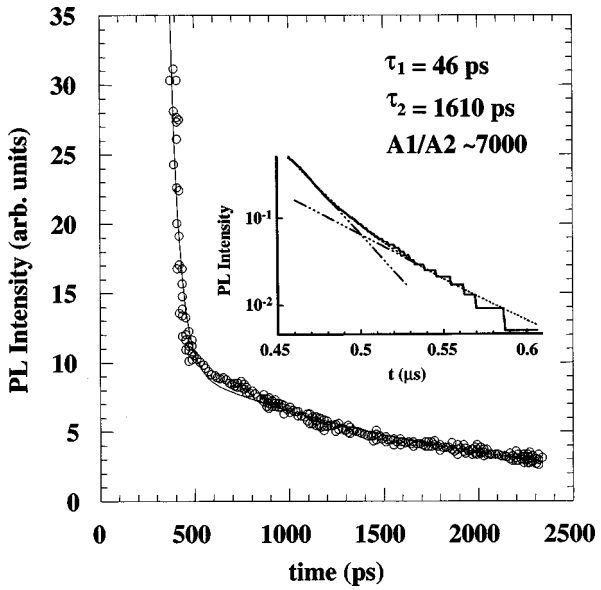

FIG. 11. Decay of the PL intensity at 460 nm for a $d=3$ nm Si nanocrystal sample. The inset shows the decay of the PL of a similar sample at lower time resolution.

To estimate the quantum efficiency (Q.E.) of various solutions of Si nanoclusters, we measured the total area under the PL curve and normalized this by the absorbance of the sample at the excitation wavelength. We performed identical measurements on a laser dye, Coumarin 500, known to be close to 100% efficient at light emission. We took the ratio of the cluster solution PL area to the dye emission PL area under identical excitation conditions, lamp energy, and spectrometer bandpass as a measure of the efficiency of light emission of the nanoclusters. The largest room temperature Q.E. achieved was 3.9% for 2.0 nm Si nanocrystals in acetonitrile with no special treatment of the cluster surface, or annealing.

In a similar study on Ge nanocrystals[19] we examined the influence of the polarity of the solvent on the Q.E. Extensive data on $d=2$ nm Ge nanocrystals revealed a gradual decrease in PL efficiency with decreasing solvent polarity (ethylene glycol>acetonitrile>toluene>orthoxylene). The same trend is expected for Si.

C. Comparison with theory

There has been an evolution of theoretical treatments of the electronic structure of semiconducting nanocrystals. The earliest treatment is the effective mass approximation (EMA) due to Efros and Efros[36] which assumed spherical nanocrystals, parabolic energy bands and infinite potential barriers at the crystal boundary. In the EMA one replaces the microscopic quasi-periodic potential of the bulk material by a constant potential, and the kinetic energy operator is replaced by an effective-mass operator derived from the parabolic expansion of the bulk band structure. Experience on a large number of materials has shown that EMA generally treats large ($d>5$–6 nm) nanocrystals fairly accurately but fails seriously for smaller nanocrystals.[37] Consequently, there have been a number of attempts at improving it. For example, Brus[38] included the electron-hole (e-h) interaction energy, i.e., the Coulomb term, dealt with finite-potential walls to

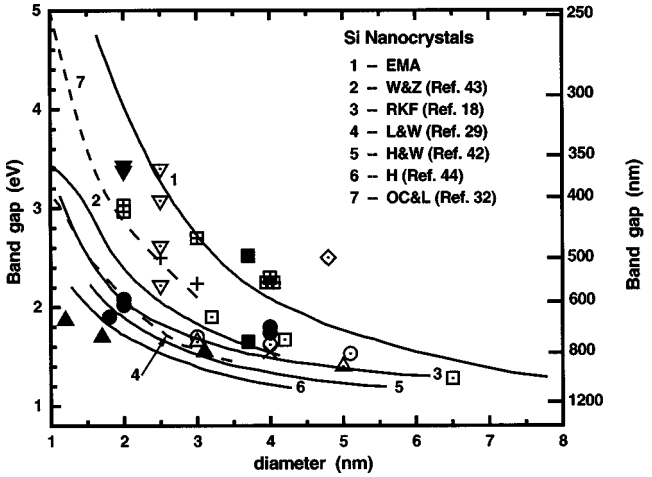

FIG. 12. Comparison of theoretical band-gap energies and experimental PL peak energies (same data as in Fig. 10) for Si nanocrystals.

calculate excited state energies, and considered the influence of the dielectric constant of the surrounding medium. Kayanuma[39] went on to consider the influence of nanocrystal shape, specifically, spheres vs cylinders. Despite these improvements, EMA results generally overestimate the confinement effect, especially for small clusters.

In an attempt to overcome this shortcoming, tight binding[40–42] and pseudopotential[18,28,43,44] methods have been employed with various degrees of success. Rama Krishna and Friesner[18] used empirical pseudopotentials to calculate the influence of size confinement on the indirect gap as well as on the $\Gamma_{25}-\Gamma_{15}$ and $\Gamma_{25}-L$ transitions. An interesting aspect of their work is the finding that the direct $\Gamma_{25}-\Gamma_{15}$ transition energy first increases slightly with decreasing crystal size and then decreases. The decrease is attributed to the inverted parabolic shape of the conduction band at Γ. Our results do not agree with this finding. Rather, we find a significant increase in this energy for our smallest nanocrystals. Another feature of their results is the finding that size confinement splits the two overlapping ($p_{\sigma*}$) conduction bands at Γ (Γ_{15}) as well as the two overlapping bands at the top of the valence band also at Γ. (Actually, these two latter bands are slightly split in bulk Si by spin-orbit interaction as shown in Fig. 3.) These splittings should, in principle, be reflected in that part of the absorption spectrum due to direct transitions at Γ. However, as we have already noted, there is no discernible evidence for it in our Si nanocrystal spectra. The reason for the absence of such evidence is embodied in the results in Fig. 3, namely the curvature of the two split-off conduction bands at Γ. Specifically, the first split-off band is concave and the second is convex providing a potential well for electrons. Thus, the first direct optical transition at Γ in Si nanocrystals is to this second band.

Figure 12 shows various theoretical results on the variation of the indirect bandgap energy with size for Si nanocrystals. Clearly, there are very substantial quantitative differences among these results, especially at small sizes making it difficult to draw any meaningful conclusions. In attempting to compare these results with experimental data, we note that very few authors have reported the experimental magnitude of the bandgap for Si clusters. Almost all of the available data consist of PL peak energies vs. size as was presented in Fig. 10. Thus, we superimpose on the theoretical results in Fig. 12 the experimental data of Fig. 10 in an attempt to look for trends. We caution, however, that many of the experimental data shown are not necessarily attributed to recombination associated with the (indirect) band gap, rather, they may be due to surface or impurity recombination or, in the case of some of our results, to direct recombination at Γ. Additionally, in comparing the experimental and theoretical results, one needs to keep in mind the relatively large and size-dependent exciton binding energy as well as the large uncertainty in determining size.

Zunger and Wang[28] compared their calculated exciton energy vs. size both with band-gaps estimated from absorption measurements and with experimental PL peak energies and found some systematic trends. Specifically, all the experimental bandgap data fell above the calculated Energy vs d curve, whereas all the PL data fell below this curve leading to the conjecture that the observed PL originates from some persistent (approximately size-independent) surface states rather than from intrinsic nanocrystal states. However, it should be noted that in this comparison the absorption and PL data came from different sources, and, furthermore, the absorption data are from porous Si samples, making definitive conclusions difficult. Although many of our findings appear to be in qualitative agreement with Zunger and Wang's observations, it is premature to come to any definitive conclusions about mechanisms. The experimental situation has to greatly improve before we reach that stage.

Leung and Whalley[29] investigated e-h interactions in truncated small spherical Si nanocrystals by incorporating Coulomb, exchange and spin-orbit couplings into tight-binding models. They reported the optical absorption spectra for nanocrystals with 41, 83, and 147 atoms in size, corresponding to $d=1.16$, 1.47, and 1.78 nm, respectively, the latter being equal in size to our smallest nanocrystals. The nanocrystals were constructed by sequentially adding shells about a central atom, and therefore have tetrahedral symmetry. Figure 13 compares their calculated $\in_2$ vs energy spectrum for the 147-atom cluster with the extinction data for our 1.8 nm nanocrystals which are of comparable size. ($\in_2$ is the imaginary part of the dielectric constant.) The absorption spectrum, $\sigma_{\rm abs}(\omega)$, is directly related to $\in_2(\omega)$ by $\sigma_{\rm abs}\sim\omega \in_2(\omega)$. The agreement between the two spectra in Fig. 13 is fairly good, especially with respect to the bandgap and the first direct ($\Gamma_{25}-\Gamma_{15}$) transition.

Several groups have calculated the intrinsic recombination rate, $1/\tau$, as a function of size using different models for band gap recombination in Si nanocrystals. Some of these results are summarized in Fig. 14 which also shows our experimental results as well as those of other authors. Because of aforementioned uncertainties in the experimental data, particularly in size determination, it had been hoped that model calculations will provide guidance as to the dependence of τ on size. Unfortunately, the very large disparities among the various model results in Fig. 14 do not allow us to draw any definitive conclusion. The only certainty in these results is that τ decreases with decreasing cluster size, as is expected. Leung and Whaley[29] provided two bounds for τ vs d as shown by the dot-dash curves. The bounds account for variations in model parameters for both surface-truncated

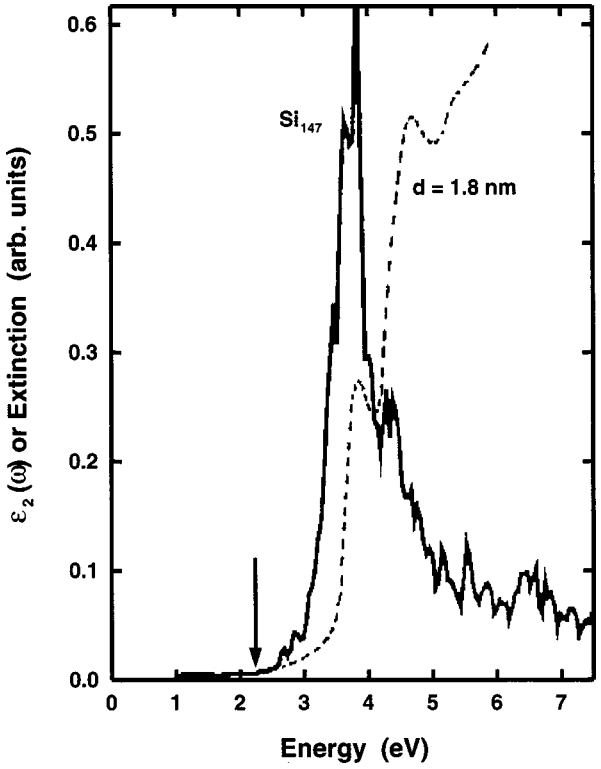

FIG. 13. Comparison of the extinction spectrum for a $d = 1.8$ nm Si nanocrystal sample with the calculated $\varepsilon_2(w)$, spectrum for 147-atom Si nanocrystals (from Ref. 29). The two nanocrystal samples are of about the same size. The arrow indicates the location of the calculated indirect band gap which is in good agreement with our experimental value.

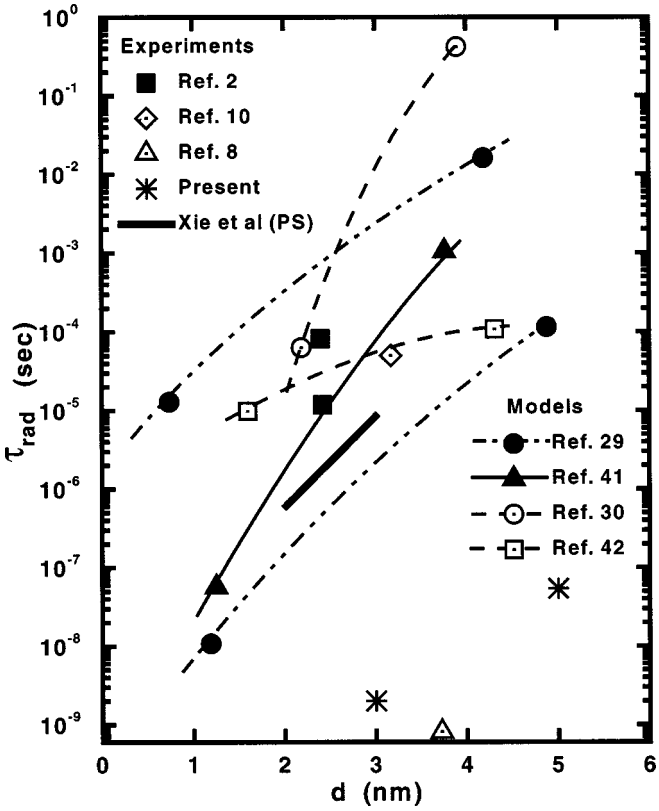

FIG. 14. Summary of the available (present work and literature) data on the dependence of the PL decay lifetime on Si nanocrystal size. Theoretical results are also shown.

and hydrogen-terminated nanocrystals. Most all of the other calculated results fall between these two bounds.

As for the experimentally determined τ's, we can make the following observations. First we note that the model results in Fig. 14 are for band gap recombination. Three data points on SiO_2-capped Si nanocrystals (one from Wilson *et al.*[10] and two, presumably on the same sample, from Littau *et al.*[2]) fall in the middle of the band of model results. The associated τ's are on the order of a few tens of microseconds. We also show a band of experimental results[1] on porous Si. These data also fall within the broad band of model results. Our two data points (τ's$=1.5$ and ~ 50 ns) and Kanemitsu's datum point ($\tau = 0.8$ ns) fall well outside the range of the model results as they should, consistent with our interpretation of the associated PL as being due to direct *e-h* recombination and surface/defect recombination and not due to bandgap recombination. There are no model calculations appropriate for these data.

IV. SUMMARY AND CONCLUSIONS

We have successfully grown size-selected Si nanocrystals in the size range 1.8 to 10 nm. HRTEM fringe images show that the nanocrystals are of high crystalline quality, and electron diffraction results show that they retain their bulk diamond structure down to about 4–5 nm diameter. Optical absorption data suggest that these nanocrystals retain their bulklike properties and structure down to the smallest sizes produced (~ 1.8 nm diameter containing about 150 Si atoms). HPLC techniques with on-line optical and electrical diagnostics were developed to purify and size separate the clusters and to ensure obtaining background-free absorbance and PL spectra.

In addition to the long wavelength absorption tail associated with the indirect-bandgap, several direct transitions were evident in the data. It was found that the smallest gap in nanosize Si remains indirect to the smallest sizes studied, $d = 1.8$ nm. The different electronic transitions exhibited various quantum confinement effects. The indirect band-gap shifts from 1.1 eV in the bulk to ~ 2.1 eV for nanocrystals ~ 2 nm in diameter (in qualitative agreement with theoretical preductions), and the direct transition at Γ ($\Gamma_{25} - \Gamma_{15}$) blue shifts by 0.4 eV from its 3.4 eV bulk value over the same size range. Some transitions were relatively insensitive to cluster size, a feature that can be qualitatively understood in terms of the shape of the associated dispersion curves in the band structure.

We have observed room-temperature photoluminescence from Si nanocrystals at various wavelengths in the range 700–350 nm (1.8–3.5 eV), i.e., across the visible range. The largest quantum efficiencies were $\sim 4\%$ for $d = 2$ nm Si. No post synthesis surface treatment was employed to achieve these results. Solvent polarity was shown to influence quantum efficiency.

The most intense PL was in the blue region of the spectrum (~ 365 nm) and is attributed it to direct electron-hole recombination at Γ ($\Gamma_{25} - \Gamma_{15}$ transition). The short radiative lifetime for this PL ($t = 1.5$ ns with a faster initial component) is comparable to that for GaAs and is consistent with

our assignment. This observation of direct recombination in Si is a consequence of quantum confinement. A relatively strong PL centered around 580 nm is fairly insensitive to cluster size, and is attributed to surface (or defect) recombination. Other PL peaks were tentatively assigned, but more work is needed to confirm the assignments.

The work presented here represents an exploratory attempt to understand the relationship between Si nanocluster size, structure, surface chemistry and the resulting optical properties. We have identified features in the optical properties that deserve much more detailed study in order to understand the influence of size and of surface bonding and termination on the electronic properties. In this regard, HPLC, which is very sensitive to small changes in surface characteristics, may play a significant role in elucidating the influence of surface structure on the optical properties of nanoclusters.

ACKNOWLEDGMENTS

This work was supported by the Division of Materials Sciences, Office of Basic Energy Sciences, U.S. Department of Energy, and by a Laboratory Directed R&D project under Contract No. DE-AC04-AL8500. Sandia is a multiprogram laboratory operated by Sandia Corporation, a Lockheed Martin Company, for the Department of Energy.

[1] See, e.g., S. S. Iyer and Y. H. Xie, Science **260**, 40 (1993), and references therein.

[2] (a) K. A. Littau, P. J. Szajowski, A. J. Muller, A. R. Kortan, and L. E. Brus, J. Phys. Chem. **97**, 1224 (1993); (b) L. E. Brus, P. F. Szajowski, W. L. Wilson, T. D. Harris, S. Schuppler, and P. H. Citrin, J. Am. Chem. Soc. **117**, 2915 (1995), and references therein.

[3] H. Takagi, H. Ogawa, Y. Yamazaki, A. Ishizaki, and T. Nakagiri, Appl. Phys. Lett. **56**, 2379 (1990).

[4] M. Yamamoto, K. Hayashi, K. Tsunetomo, K. Khono, and Y. Saka, Jpn. J. Appl. Phys., Part 1 **30**, 136 (1991); Y. Osaka, K. Tsunetomo, F. Toyomura, H. Myoren, and K. Kohno, Jpn. J. Appl. Phys., Part 2 **31**, L565 (1992).

[5] W. A. Saunders, P. C. Sercel, R. B. Lee, H. Atwater, K. J. Vahala, R. C. Flanagan, and E. J. Escorsi-Aparcio, Appl. Phys. Lett. **63**, 1549 (1993).

[6] S. Iwasaki, T. Ida, and K. Kimura, Jpn. J. Appl. Phys., Part 2 **35**, L551 (1996).

[7] S. H. Risbud, L. C. Liu, and J. F. Shackelford, Appl. Phys. Lett. **63**, 1648 (1993).

[8] Y. Kanemitsu, Phys. Rev. B **49**, 16 845 (1994).

[9] C. W. White, S. P. Withrow, A. Meldrum, J. D. Budai, D. M. Hembree, J. G. Zhu, D. O. Henderson, and S. Prawer (unpublished); see also J. Appl. Phys. **78**, 4386 (1995).

[10] W. L. Wilson, P. F. Szajowski, and L. E. Brus, Science **262**, 1242 (1993).

[11] A. P. Alvisatos, Mater. Res. Bull. **19**, 23 (1995) and references therein.

[12] J. P. Wilcoxon, U.S. Patent No. 5147841 (15 September 1992).

[13] J. P. Wilcoxon, R. L. Williamson, and R. J. Baughman, J. Chem. Phys. **98**, 9933 (1993).

[14] J. P. Wilcoxon and G. A. Samara, Phys. Rev. B **51**, 7299 (1995); see also J. P. Wilcoxon, P. P. Newcomer, and G. A. Samara, Solid State Commun. **98**, 581 (1996).

[15] J. P. Wilcoxon and S. A. Craft, *NanoStructured Materials* (Elsevier Science Ltd., Amsterdam, 1997), Vol. 9, pp. 85–88.

[16] See, e.g., S. M. Sze, *Physics of Semiconductor Devices* (Wiley-Interscience, New York, 1969), Chap. 2, and references therein.

[17] M. L. Cohen and T. K. Bergstresser, Phys. Rev. **141**, 789 (1966).

[18] M. V. Rama Krishna and R. A. Friesner, J. Chem. Phys. **96**, 873 (1992).

[19] J. P. Wilcoxon and G. A. Samara (unpublished).

[20] J. R. Heath, J. J. Shiang, and A. P. Alivisatos, J. Chem. Phys. **101**, 1607 (1994).

[21] See, e.g., J. I. Pankove, *Optical Processes in Semiconductors* (Dover, New York, 1975), Chap. 2.

[22] M. F. Jarrold and V. A. Constant, Phys. Rev. Lett. **67**, 2994 (1991).

[23] E. Kaxiras and K. Jackson, Phys. Rev. Lett. **71**, 727 (1993).

[24] U. Rothlisberger, W. Andreoni, and M. Parrinello, Phys. Rev. Lett. **72**, 665 (1994).

[25] K. D. Rinnen and M. L. Mandich, Phys. Rev. Lett. **69**, 1823 (1992).

[26] N. Binggeli and J. R. Chelikowsky, Phys. Rev. Lett. **75**, 493 (1995).

[27] J. R. Haynes and W. C. Westphal, Phys. Rev. **101**, 1676 (1956).

[28] A. Zunger and L. W. Wang, Appl. Surf. Sci. **102**, 350 (1996).

[29] K. Leung and K. B. Whaley, Phys. Rev. B **56**, 7455 (1997).

[30] T. Takagahara and K. Takeda, Phys. Rev. B **46**, 15 578 (1992).

[31] See, A. J. Read, R. J. Needs, K. J. Nash, L. T. Canham, P. D. J. Calcott, and A. Qteish, Phys. Rev. Lett. **69**, 1232 (1992); T. Ohno, K. Shiraishi, and T. Ogawa, *ibid.* **69**, 2400 (1992).

[32] (a) S. Ögüt, J. R. Chelikowsky, and S. G. Louie, Phys. Rev. Lett. **79**, 1770 (1997); (b) We are thankful to Professor L. E. Brus for emphasizing this point.

[33] G. Allan, C. Delerue, and M. Lannoo, Phys. Rev. Lett. **76**, 2961 (1996).

[34] S. Schuppler, S. L. Friedman, M. A. Marcus, D. L. Adler, Y. H. Xie, F. M. Ross, T. D. Harris, W. L. Brown, Y. J. Chabal, L. E. Brus, and P. H. Citrin, Phys. Rev. Lett. **72**, 2648 (1994).

[35] (a) K. Kim, Phys. Rev. B **57**, 13 072 (1998); (b) Y. Kanemitsu, H. Uto, and Y. Masumoto, *ibid.* **48**, 2827 (1993); (c) P. Li, G. Wang, Y. Ma, and R. Fang, *ibid.* **58**, 4057 (1998); (d) G. G. Qin, X. S. Liu, S. Y. Ma, J. Lin, G. Q. Yao, X. Y. Lin, and K. X. Lin, *ibid.* **55**, 12 876 (1997).

[36] Al. L. Efros and A. L. Efros, Fiz. Tekh. Poluprovodn. **16**, 6209 (1982) [Sov. Phys. Semicond. **16**, 772 (1982)].

[37] See, e.g., A. D. Yoffee, Adv. Phys. **42**, 173 (1993) for a review.

[38] L. E. Brus, J. Chem. Phys. **79**, 5566 (1983); **80**, 4403 (1984).

[39] Y. Kayanuma, Phys. Rev. B **38**, 9797 (1988); **44**, 13 085 (1991).

[40] Y. Wang and N. Herron, J. Phys. Chem. **91**, 257 (1987); **92**, 4988 (1988).

[41] P. E. Lippens and M. Lannoo, Phys. Rev. B **39**, 10 935 (1989); **41**, 6079 (1990).

[42] N. A. Hill and K. B. Whaley, Phys. Rev. Lett. **75**, 1130 (1995).

[43] L. W. Weng and A. Zunger, J. Phys. Chem. **100**, 2394 (1994), and references therein.

[44] M. S. Hybertsen, Phys. Rev. Lett. **72**, 1514 (1994), and references therein.